RSC Advances

ROYAL SOCIETY OF CHEMISTRY

www.rsc.org/advances

RSC Advances

ARTICLE

Density-Functional Studies of Hydrogen Peroxide Adsorption and Dissociation on MoO_3(100) and $H_{0.33}MoO_3$(100) Surfaces.

Received 00th January 20xx,
Accepted 00th January 20xx

DOI: 10.1039/x0xx00000x

www.rsc.org/

Evgueni B. Kadossov,[a] Ahmad Razzaghi Soufiani,[b] Allen W. Apblett[b] and Nicholas F. Materer†[b]

Hydrogen peroxide (H_2O_2) adsorption and dissociation mechanisms on MoO_3(100) and $H_{0.33}MoO_3$(100) surfaces were studied by means of density-functional computations. Mechanisms were examined on both fixed and relaxed clusters. On both fixed and relaxed molybdenum oxide clusters, H_2O_2 adsorbs molecularly and does not dissociate. However, on the surface of both the fixed and relaxed molybdenum hydrogen bronze ($H_{0.33}MoO_3$) clusters, H_2O_2 can dissociate through a pathway involving either H-O or O-O bond cleavage. The barrier for direct H-OOH dissociation is 39.9 kJ/mol, leading to an adsorbed H atom and a HOO group. The dissociation of the O-O bond leads to the most energetically stable products, two OH species bound to the surface molybdenum atoms with the relative adsorption energy - 430.4 kJ/mol. The mechanism on the relaxed cluster is slightly more complex due to additional stability of the molecularly adsorbed structure and ability to form a geminal intermediate not found on the fixed cluster. On both the relaxed and fixed clusters, hydrogen cleavage is kinetically favoured. Chemical reaction on the molybdenum hydrogen bronze surface is made possible by the increased electron density at the surface with respect to the oxide due to the contribution from the HOMO orbital.

Introduction

Molybdenum oxides, in the pure form or mixed with other metal oxides are catalytically active towards oxidation of hydrocarbons,[1-4] alcohols,[5-7] hydrocracking,[8] hydrogenation[9] and hydrodeoxygenation of aldehydes.[10] In the MoO_3 crystal, the (100) and (001) faces are responsible for hydrogen abstraction process, while nucleophilic addition of oxygen into the allylic species occurs at the (010) plane.[1, 3] The MoO_3(100) surface has Lewis acid centers that are found to be important for olefin adsorption and stabilization of intermediate species.[11] A number of experimental and theoretical studies on the bulk and surface properties of molybdenum oxides including their electronic structures have been done during the last 15 years[10, 12-19] including investigations of the decomposition of acetaldehyde,[10] the adsorption of H_2O and CO,[12] hydrogen adsorption, and allylic oxidation[20] on the (100) and (010) surfaces of MoO_3.

The reduction of MoO_3 with atomic hydrogen leads to formation of molybdenum bronzes with the general formula H_xMoO_3 ($0 \le x \le 2$). Since the average oxidation number of Mo in H_xMoO_3 is less than 6, molybdenum bronzes are strong reducing agents and have received attention as potential hydrogenation, dehydration and reduction catalysts.[21-23] Depending on the amount of hydrogen, four phases of H_xMoO_3 have been identified.[24] According to early NMR studies, the H atoms in molybdenum bronzes preferentially occupy the intralayer positions on a quasi-one dimensional zigzag line connecting the vertex-sharing oxygen atoms of the MoO_6 octahedra.[25, 26] Once these sites are saturated, hydrogen atoms supposedly start to populate the interlayer positions, coordinating to the terminal oxygen atoms. However, recent combined experimental and computational studies indicate no hydrogen population of the intralayer sites.[27] Density function theory (DFT) calculations suggest that hydrogen will bind to the symmetric bridging oxygen, the asymmetric bridging oxygen and to the terminal oxygen of the MoO_3 lattice with adsorption energies ranging from 2.10 to 2.91 eV.[28, 29] The most favourable hydrogen adsorption sites were found to be the terminal and asymmetric oxygen atoms, which interact with hydrogen atoms with almost equal bond strength. The particular hydrogen distribution in molybdenum bronzes seems to be dependent on the preparation method.

Information regarding the reaction chemistry of H_xMoO_3 is scarce. Indeed, we were unable to locate any articles discussing the

[a] Xplosafe, LLC, 1414 South Sangre Road, Stillwater, OK 74074.
[b] Department of Chemistry, Oklahoma State University, Stillwater, OK 74078.
† Corresponding Author E-Mail: materer@okstate.edu
Electronic Supplementary Information (ESI) available: Structures, Energies and coordinates of all structures can be found in the supplementary information. See DOI: 10.1039/x0xx00000x

reaction of these materials with peroxides in any detail. Relevant papers include the use of molybdenum bronzes as an agent for uranium removal, in which H_xMoO_3 reacts with uranyl ions to form the mineral iriginite, $UMo_2O_9 \cdot 3H_2O$.[30] In a similar fashion, Th, Nd and Pb ions can also be separated from water and immobilized by reaction with the bronze..[31, 32] For peroxide compounds, it was found that the molybdenum hydrogen bronze can successfully decompose triacetone triperoxide by reacting with the peroxide groups and concomitantly oxidize the molybdenum reagent turning the initial deep blue colour to yellow.[33] In this paper, we have modelled adsorption and possible decomposition of hydrogen peroxide on the MoO_3(100) and $H_{0.33}MoO_3$(100) surfaces using density-functional calculations to gain insight into the possible mechanisms for the decomposition reaction on the bronze surface.

Computational procedure

Unless noted, calculations were done with Gaussian 03 and 09 software.[34] Except when explicitly noted, simulations were performed using Becke three parameter hybrid functionals[35] with Lee, Yang and Parr correlation that includes both local and non-local terms (B3LYP).[36] The 6-311++G(d,p) valence triple zeta basis set with two diffuse functions and the polarization d-and p-functions on non-hydrogen and hydrogen atoms respectively was employed for all O and H atoms.[37, 38] The Mo atoms were modelled with the LanL2DZ basis set, which includes the D95 double-zeta basis set, combined with the Los-Alamos effective core potentials.[39-41] In some cases other DFT functionals and basis sets were also employed. In all cases, the wavefunction was checked for stability due to difficulties observed during optimizations. In addition, vibrational frequency analysis was performed for each configuration to confirm that all stable structures have no imaginary modes and all transition states possess exactly one negative normal mode. The intrinsic reaction coordinate method was utilized to confirm that the computed transition state connects the respective reagent to the correct product.

The MoO_3(100) surface was represented by clusters containing either six or ten Mo atoms, while the Phase I molybdenum bronze(100) or $H_{0.33}MoO_3$ (100) surface was built from the smaller six atom cluster (Figure 1). A cluster approach was motivated by our emphasis on the localized adsorption and dissociation of the peroxides. In forming the clusters, all dangling bonds were terminated with either an H atom or an OH group to maintain the correct oxidation states of the Mo atoms. For the MoO_3 (100) surface, the resulting cluster models are $Mo_6O_{23}H_{10}$ and $Mo_{10}O_{36}H_{12}$ (Figures 1A and 1B). There are four phases of hydrogen molybdenum bronzes with general H_XMoO_3 formula that have been reported [24]. Depending on the amount of hydrogen, the hydrogens first attach to asymmetric bridging oxygen atoms, and then start to attach to terminal oxygen atoms. For the $H_{0.33}MoO_3$ bronze, all protons are attached to asymmetric bridging oxygen atoms. [42] Thus, the $H_{0.33}MoO_3$(100) surface was created by adding an H atom to each of the two asymmetric bridging oxygen atoms of the $Mo_6O_{23}H_{10}$ clusters (Figure 1C). Without including the terminating H and OH groups, the resulting ratio between the additional hydrogen and molybdenum atoms is 1:3, the correct stoichiometry for the bronze.

Small clusters of transition metal oxides typically are very highly ionic and require geometric constraints for stability. The optimizations were performed by allowing the hydrogen peroxide (H_2O_2) to first relax while keeping the geometric parameters of the MoO_3 and $H_{0.33}MoO_3$ clusters fixed at values obtained from the experimental geometries of either molybdenum trioxide[43] or hydrogen molybdenum bronze.[26, 42] Once the optimal geometry was obtained on the fixed cluster, the surface atoms (Mo and O), and the O atoms in the –OH capping groups at the surface were relaxed along the surface normal. In addition, all terminating H and O atoms and remaining terminating OH groups were fully optimized in all directions. For the hydrogen molybdenum bronze, the optimization included the two H atoms attached to the asymmetric bridging oxygen atoms. Except when noted, the results reported are obtained by this two-step optimization. Section 1 of the Supplemental Information provides more information on the optimization procedure and Section 2 contains the optimal geometries for the oxide and bronze structures. The degree of optimization in this paper is significantly greater than that typically employed for metal oxide clusters. For example, more restrictive partial optimizations were used in two other studies examining adsorption of NO and NH_3 on the MoO_3(010) surface, respectively.[44, 45]

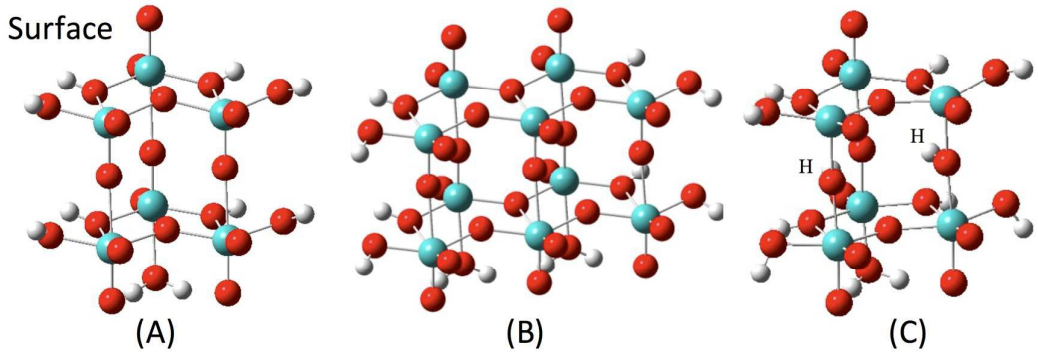

Figure 1: The $Mo_6O_{23}H_{10}$ (A) and $Mo_{10}O_{36}H_{12}$ (B) clusters used to represent the MoO_3(100) surface. The $H_{0.33}MoO_3$(100) surface is represented by a cluster (C) formed by adding two H atoms to the $Mo_6O_{23}H_{10}$ cluster (A). The Mo atoms are represented by larger blue spheres, the O atoms by red ones and the H atoms by small white spheres. Given the size of structure (B), the cluster was fixed during the optimization.

Finally, the adsorption energy was computed as the difference between the total electronic energy of the adsorption model and the isolated molecule and cluster. The basis set superposition error (BSSE)[46] correction was calculated for all structures using the standard counterpoise procedure built into the Gaussian 03 and 09 code. For the fixed clusters, the zero-point energy correction is small and effectively cancels out when calculating the adsorption energies on the surface. This correction to the relaxed structures is small (between 2% and 10% on selected structures). Thus, this correction was not included.

Results and discussion

Method Validation

Geometry optimization of an isolated H_2O_2 molecule was performed using the 6-311++G(d,p) basis set with B3LYP and *ab initio* methods (MP2 and CCSD(T)). All optimized geometries were very close to the experimental results.[44, 45] For the B3LYP functional, the difference between the computed and experimental bond lengths is only 0.002 Å and the calculated ∠OOH angles are only 0.5° larger than experimental results. To further test the applicability of the selected computational method to the hydrogen peroxide adsorption on the MoO_3 surface, H_2O_2 adsorption was modelled on a small MoO_5H_4 cluster using B3LYP and *ab initio* MP2 as well as CCSD(T) with a 6-311++G(d,p) basis set. The CCSD(T) calculation was a single-point computation at the B3LYP optimized geometry. The adsorption energies calculated with MP2 and CCSD(T) were within 3.2 kJ/mol and 5 kJ/mol, respectively, of the DFT results. A B3LYP computation with a much larger aug-cc-pVTZ basis set,[47, 48] which includes the aug-cc-pVTZ-PP basis set for Mo atom, [49] was within 2.8 kJ/mol of the 6-311++G(d,p) results. This basis set was previously utilized to adequately simulate the potential energy surfaces for hydrolysis of molybdenum oxide clusters[50] indicating that the chosen functional and the basis set are sufficient for our computations. The chosen level is consistent with a $Mo_{15}O_{56}H_{22}$ cluster study Tokarz-Sobieraj et al.[19] and a Mo_3O_9 study by Pudar et al.[51] It is also consistent with studies examining the hydrodeoxygenation of acrolein,[52] NH_3 adsorption[44] and NO adsorption[45] on MoO_3 cluster models.

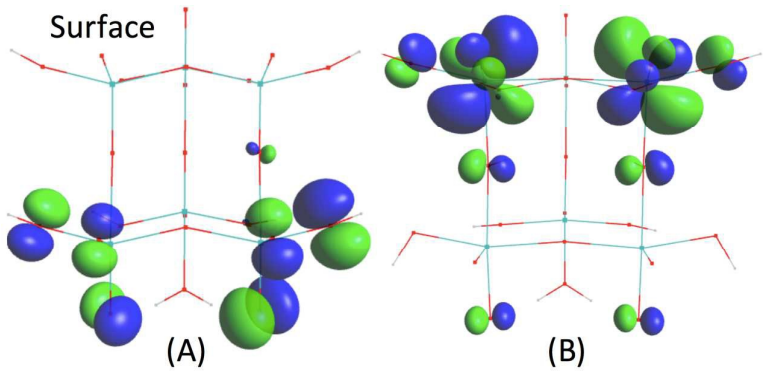

Figure 2: The computed HOMO for the $Mo_6O_{23}H_{10}$ cluster (A) and for the $Mo_6O_{23}H_{12}$ cluster (B). For clarity, a wireframe is used for the molecular structure.

Electronic structure of the MoO_3 and $H_{0.33}MoO_3$ model clusters

The highest occupied molecular orbital (HOMO) of the MoO_3(100) surface, modelled by the $Mo_6O_{23}H_{10}$ cluster (Figure 2A), shows almost no electron density on the surface molybdenum or oxygen atoms, indicating low likelihood for surface covalent bonding with an incoming adsorbate. The lowest unoccupied molecular orbital (LUMO) of the same clusters is comprised primarily of empty *d* orbitals on the surface molybdenum atoms. These empty *d* orbitals suggest that adsorption can occur via formation of a dative bond between the empty orbital and an oxygen lone pair on the H_2O_2 molecule. The addition of two hydrogen atoms to the bridging oxygen atoms of the $Mo_6O_{23}H_{10}$ cluster, forming a bronze, (Figure 1C) dramatically changes its surface reactivity and electronic structure. Unlike MoO_3, the HOMO of the molybdenum bronze cluster (Figure 2B) shows significant electron density on the two surface Mo atoms, which corresponds to the Mo 3*d* unpaired electrons. These electrons are extremely reactive and possibly could produce strong covalent bonds with the products of HOOH dissociation. As in the oxide, the LUMO of the bronze is also comprised primarily of empty Mo 3*d* orbitals with some contributions from the O 2*p* orbitals indicating the possibility of dative bond formation with an adsorbed H_2O_2 species.

Possible molecular adsorption configurations of H_2O_2 on the MoO_3(100) surface are shown in Figure 3 and summarized in Table 1. Section 3 of the Supplemental Information contains the optimal geometries and energies of all stable structures and transition states. As discussed above, the H_2O_2 can molecularly adsorb on a $Mo_6O_{23}H_{10}$ cluster through the lone pairs of the oxygen atoms. There are two possible geometries. The non-bonding oxygen atom can either face away from the cluster (Figure 3A) or into the cluster (Figures 3B and C). The first configuration (HOOH1) contains one hydrogen bond formed between a peroxide hydrogen atom (H_1) and lattice oxygen atom, while the second (HOOH2) has both hydrogen atoms on the peroxide forming hydrogen bonds with oxygen atoms of the cluster. This extra hydrogen bonding in the HOOH2 structure results in it having an adsorption energy that is slightly more exothermic or favourable than HOOH1 by 9.2 kJ/mol (see Table 1).

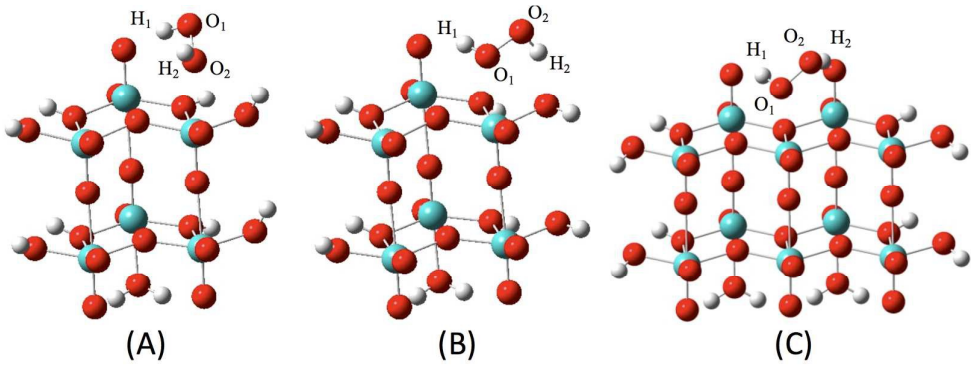

Figure 3: Molecule adsorption geometries for H_2O_2 on the $Mo_6O_{23}H_{10}$ cluster, HOOH1 (A) and HOOH2 (B). HOOH3 (C) is an additional structure found for the larger $Mo_{10}O_{36}H_{12}$ cluster. Due to the size of (C), the cluster was fixed during the optimization.

Table 1. B3LYP/LanL2DZ + 6-311++G(d,p) optimized adsorption bond lengths (Å) and energies (kJ/mol) for H_2O_2 absorption on model MoO_3 (100) surface. The parameters for H_2O_2 are included for comparison. Geometrical models for these surfaces are shown in Figures 3 and 4. The $Mo_6O_{23}H_{10}$ structures were obtained using relaxed clusters, while the larger clusters, given their size, were fixed (see text).

Model	d_{Mo-O}	d_{O1-O2}	d_{O1-H1}	d_{O2-H2}	$d_{O(lat)-H1}$	$d_{O(lat)-H2}$	E_{ads}
Absorbate							
H_2O_2		1.454	0.967	0.967			
$Mo_6O_{23}H_{10}$							
HOOH1	2.528	1.442	0.981	0.969	1.866		-41.8
HOOH2	2.464	1.446	0.976	0.983	2.077	1.824	-51.0
$Mo_{10}O_{36}H_{12}$							
HOOH1	2.426	1.446	0.984	0.968	1.836		-69.0
HOOH2	2.425	1.449	0.981	0.983	2.022	1.847	-74.1
HOOH3	2.422	1.437	0.980	0.984	1.983	1.808	-80.6
HO-OH1	2.210		0.975	0.975	2.181	2.159	+275.7*

*BSSE correction was not computed for this structure

In both cases, one of the O atoms of the H_2O_2 forms a dative bond with a Mo-O bond length of approximately 2.53 and 2.46 Å, respectably. This value is close to the Mo-O dative bond length of 2.487 Å obtained from DFT calculations for H_2O adsorption on MoO_3 surface.[53] Comparing these adsorbed structures to the gas phase H_2O_2 species, one finds that the O-H bonds involved in H bonding are slightly elongated. The O-H bond length remains very close to that in the gas phase results for the non-hydrogen

bonding peroxide hydrogen atom for both configurations. However, the H bonding results in a slightly shorter O-O bond length than in the gas-phase peroxide, implying that the H bond is responsible for a significant faction of the adsorption energy. Since a typical value of O-H ··· O hydrogen bond strength in water is 23.4 kJ/mol[54] the total contribution of hydrogen bonding to the resulting adsorption energy is approximately 40% (see Table 1).

Since the adsorption process for HOOH1 and HOOH2 creates new adsorbate-surface bonds without dissociation, the adsorption is expected to be barrierless. A set of optimizations was performed as a function of the Mo-O bond length to simulate the approach of the H_2O_2 molecule to the surface. No barrier was observed for either structure. The conversion of less favourable HOOH1 to HOOH2 by rotation around the Mo-O bond requires the breaking of one H bond. There are two transition states formed by rotation either counter-clockwise or clockwise with respect to the HOOH1 structure. These transitions states are labelled TS1-Oxide and TS2-Oxide, respectively, in the Supplemental Information, Section 2. The rotational barriers are 10.3 and 14.8 kJ/mol, depending on the rotation direction, and are consistent with the breaking of a hydrogen bond during the rotation.

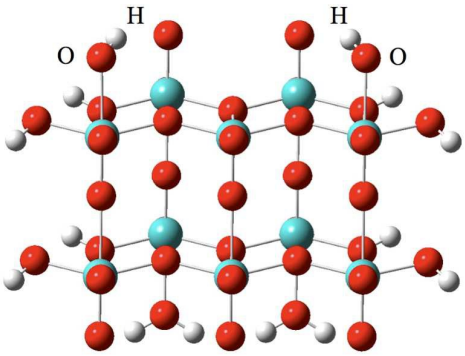

Figure 4: The $Mo_{10}O_{36}O_{12}$ cluster with two adsorbed OH groups (HO-OH1). Given the size of this structure, the cluster was fixed during the optimization.

The effect of surface relaxation (optimization of the cluster) on the energetics can be inferred by comparing the final results with those initial results obtained using a fixed $Mo_6O_{23}H_{10}$ cluster. In both case, a reduction in the adsorption energies by approximately 20 kJ/mol is observed for both HOOH1 and HOOH2 structure, with respect to the fixed cluster. This decrease is attributed to an increase in intracluster binding leading to a decrease in the electron density available to form additional chemical binds with the adsorbate. It is possible to allow the terminal –OH groups to fully relax (see Section 1 of the Supplemental Information for information on the optimization procedure). Such optimizations result in these groups moving further upward, with the terminal oxygen atoms now in unrealistic positions with respect to that expected for an extended surface. In addition, the adsorption energy of both HOOH structures and the magnitude of the transition barrier (TS1) decreased by several kJ/mol due to the resulting steric repulsion. Thus, full optimizations of the terminal–OH groups at the surface were not performed for all further computations.

To examine possible size effects, computations were performed on a larger $Mo_{10}O_{36}H_{12}$ cluster with ten Mo atoms. For this large cluster, the cluster atoms were fixed at the experimental positions. When compared to an optimization on the smaller cluster with cluster atoms fixed at the experimental positions, there was practically no difference in the adsorption energies. There was less than 5 kJ/mol difference between the HOOH1 (Figure 3A) and HOOH2 (Figure 3B) configurations on $Mo_6O_{23}H_{10}$ and $Mo_{10}O_{36}H_{12}$ clusters. Thus, the effect of cluster size is minimal due to the localized bonding in these oxides. Another configuration, HOOH3 (Figure 3C), is possible on the larger $Mo_{10}O_{36}H_{12}$ cluster. This configuration forms a dative bond from the central Mo to one of the H_2O_2 O atoms and two H bonds to the lattice O atoms. With the exception of one of the H bonds being to a surface O atom instead of a lattice O atom, this structure is very similar to HOOH2. Indeed, the adsorption energy of this new geometry, again with the cluster atoms fixed due to the size, is only 8.0 kJ/mol lower than that computed for HOOH2 on the smaller $Mo_6O_{23}H_{10}$ cluster. This result is attributed to the localized nature of bonding in the oxide cluster. Given these results, we utilized the smaller cluster for all further computations

The possibility that H_2O_2 dissociation occurs on the MoO_3(100) surface was also investigated. In general, there can be two possible bond-breaking mechanisms. The first involves hydrogen abstraction and results in adsorbed OOH and H. However, no stable structures could be found on the $Mo_6O_{23}O_{10}$ cluster for trial geometries with the H atom attached to a surface O atom. In the O-O bond cleavage mechanism, the reaction results in two absorbed OH groups. Again, no stable structures could be found for geometries with adjacent OH groups. A stable geometry with the two OH groups on opposite sides of the larger $Mo_{10}O_{36}H_{12}$ cluster (Figure 4) could be found. However, the computed adsorption energy (275.7 kJ/mol) was positive, indicating that

adsorption is energetically unfavorable. Thus, the dissociation of H_2O_2 on MoO_3(100) is not feasible and only molecular adsorption is expected. These results are consistent with the HOMO (Figure 2A) providing limited electron density at the surface.

Table 2. B3LYP/LanL2DZ + 6-311++G(d,p) optimized adsorption bond lengths (Å) and energies (kJ/mol) for H_2O_2 absorption on the $H_{0.33}MoO_3$ (100) surface. Geometrical models for these surfaces are shown in Figures 5, 6, and 7. All optimizations were performed allowing the surface of cluster to relax (see text).

Model	d_{Mo-O}	d_{O1-O2}	d_{O1-H1}	d_{O2-H2}	$d_{O(lat)-H}$	E_{ads}
HOOH1	2.181	1.442	0.991	0.970	1.762	-105.9
HOOH2	2.188	1.452	0.988	0.991	1.926	-119.6
HOO-H1	1.956	1.433	0.981		0.976	-110.0
HOO-H2	1.884	1.384	0.998		1.670	-25.4
HO-OH2	1.866		0.981	0.972	1.959	-430.4
HO-OH3	1.971		0.965	0.997		-109.2
HO-OH4	1.980	2.306	0.969	0.969		-212.0
HO-OH5	1.870		0.980	0.965	2.066	-414.5

Table 3. Transition states optimized adsorption bond lengths (Å) and energies (kJ/mol) for H_2O_2 on the $H_{0.33}MoO_3$ (100) surfaces. Pathways scheme for the absorption and dissociation of H_2O_2 on the $H_{0.33}MoO_3$ is shown in Figure 8 with reaction energetics shown in Figure 9. Geometrical models for these surfaces can be found in the Supplemental Information. **A**ll optimizations were performed allowing the surface of the cluster to relax (see text).

Model	d_{Mo-O}	d_{O1-O2}	d_{O1-H1}	d_{O2-H2}	$d_{O(lat)-H}$	E_{ads}
TS1	2.265	1.438	0.977	0.972	2.199	-67.4
TS2	2.257	1.451	0.976	0.971		-74.2
TS3	2.351	1.462	1.410	0.974		+145.2
TS4	1.902	1.401	0.995		1.551	+115.7
TS5	2.091	1.446	1.286	0.983	1.195	-79.7
TS6	1.915	2.192	0.966	0.973		+18.2
TS7	1.893		0.980	0.970	2.004	-36.9
TS8	2.158	1.850	0.973	0.977	2.244	+6.7
TS9	1.922		0.969	0.968		-151.1
TS10	1.873		0.978	0.960	2.075	-407.2

H_2O_2 adsorption and dissociation on the $H_{0.33}MoO_3$(100) surface

Similar to that of the MoO_3(100) surface, the LUMO for the $H_{0.33}MoO_3$(100) surface contains empty Mo 3*d* orbitals that can form a dative bond with an oxygen lone pair from the H_2O_2 molecule. However, the presence of surface density from the HOMO implies that covalent bonds are also possible. Computations were performed starting with the HOOH1 and HOOH2 geometries obtained from the oxide surface. The dissociation of the H_2O_2 can lead to several structures containing adsorbed H atoms, OOH and OH groups. These dissociative structures are shown in Figures 5, 6 and 7. The overall reaction scheme and computed reaction pathway energetics are shown in Figures 8 and 9, respectfully. The stable structures are reported in Table 2, while the transition state energies are tabulated in Table 3. Section 4 of the Supplemental Information contains the optimal geometries and energies of all stable structures and transition states.

For the HOOH1 configuration, an analogous molecular adsorption configuration is found on the $H_{0.33}MoO_3$ cluster. However, the adsorption energy (-105.9 kJ/mol) is 64.1 kJ/mol lower than that found for the $Mo_6O_{23}H_{10}$ clusters. This lower energy is reflected in the significant contraction of the Mo-O adsorption bond length, which is shorter for the Mo bronze by 0.35 Å (Table 2). Since the adsorption process for HOOH1 involves no bond breaking, the adsorption is expected to be barrierless. To confirm this expectation for the oxide clusters, the adsorption pathway for this structure was simulated by a set of optimizations performed as a function of the Mo-O bond length, in effect bringing the H_2O_2 species slowly towards the surface, and no barrier was observed. In addition, similar to what was found for the MoO_3 cluster, the HOOH1 structure can convert into a slightly more stable HOOH2 configuration.

All attempts to perform geometry optimization on the analogous HOOH2 adsorption configuration using a fixed cluster failed. Computations of the HOOH2 geometry with the Mo-O bond constrained perpendicular to the surface and the cluster fixed, led to a stable structure with a negative adsorption energy of -108.8 kJ/mol. A possible barrier to dissociation was investigated by simulating the adsorption process by a set of optimizations performed as a function the Mo-O bond length to bringing the H_2O_2 species slowly towards the surface. No barrier was observed. Once the cluster is allowed to relax, the optimal distance between the lattice or surface oxygen and hydrogen atom of the H_2O_2 increases, allowing a stable species to be located. The adsorption

energy of this structure is -119.6 kJ/mol, which is not too different from the -108.8 kJ/mol value estimated using the fixed cluster. The increased absolute value of absorption energy of HOOH2 with respect to the oxide surface is reflected in the significant contraction of the Mo-O adsorption bond length by 0.28 Å (Table 2). Finally, the adsorption energy is lower than that for the HOOH1 geometry. Similar to the oxide clusters, this reduction is attributed to additional hydrogen bonding with the lattice oxygen.

HOOH1 and HOOH2 configurations on the $H_{0.33}MoO_3$ (100) surface can interconvert through two transition states (TS1 and TS2) corresponding to clockwise and counter-clockwise rotation of the molecularly adsorbed HOOH species. The transition barrier magnitudes are 38.5 kJ/mol in case of clockwise rotation (TS1) and 31.7 kJ/mol for the counter-clockwise rotation (TS2). The interconversion barriers are approximately 20 to 25 kJ/mol more than the corresponding barrier on the MoO_3(100) cluster.

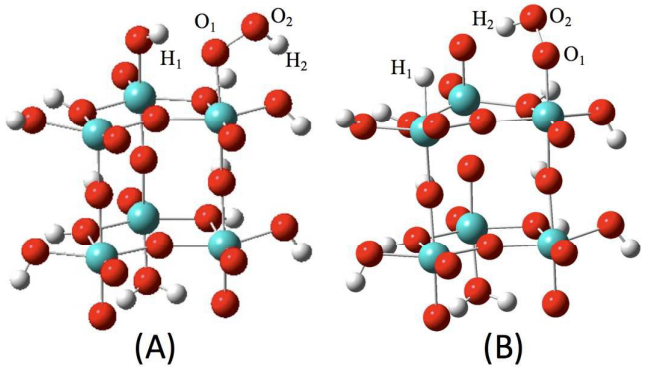

Figure 5: Dissociation formed by O-H bond cleavage on the $H_{0.33}MoO_3$(100) surface. Structure (A) results from an H atom migrating to an O atom (HOO-H1), and (B) results from the hydrogen migration to a surface molybdenum atom (HOO-H2).

Starting from either of the two molecularly adsorbed structures (HOOH1 or HOOH2), there is both a direct and an indirect hydrogen abstraction pathway (see Figures 8 and 9) to form HOO-H1 (Figure 5A). Once HOOH2 forms, an H atom from the H_2O_2 can migrate to a lattice O atom over a barrier of 39.9 kJ/mol (TS5). Thus, HOO-H1 is easily accessible. On the relaxed structures, HOO-H1 is less stable than HOOH2 by about 10 kJ/mol. With a fixed or unrelaxed cluster, the opposite is true. Given that the relaxed cluster may overestimate the flexibility possible in an extended system and the small energy difference between HOOH2 and HOO-H1, we expect that both HOOH2 and HOO-H1 could both co-exist on the bronze surface. The indirect hydrogen abstraction pathway starts with HOOH1 and involves the migration of a hydrogen atom over a relatively large (251.1 kJ/mol) barrier (TS3) to a surface molybdenum atom forming an intermediate state (HOO-H2). This configuration is shown in Figure 5B. Given that the Mo-H bond is relatively weak (bond length of 1.679 Å), the relative stability of this structure with respect to the molecular species is due to the hydrogen atom forming a strong hydrogen bond with the surface lattice oxygen (bond length of 1.670 Å). As in the case of HOO-H1, there is significant contraction of the Mo-O bond length, in this case from 2.18 to 1.88 Å, indicating a strong chemical bond with the OOH species. However, the barrier (251.1 kJ/mol) is significantly larger than the adsorption energy (-105.9 kJ/mol). In addition, the adsorption energy of this intermediate (HOO-H2) is -25.4 kJ/mol, larger than either the HOOH1 or HOOH2 configuration. A similarly large energy barrier is also found for the fixed cluster. In the unlikely event that this intermediate forms, the same final structure (HOO-H1) as that found for the direct pathway can be obtained by passing through a 141.1 kJ/mol barrier (TS4). The large transition state barrier (TS3) found on both the relaxed and fixed clusters with respect to the adsorption energy, makes the indirect H dissociation energetically unfavorable.

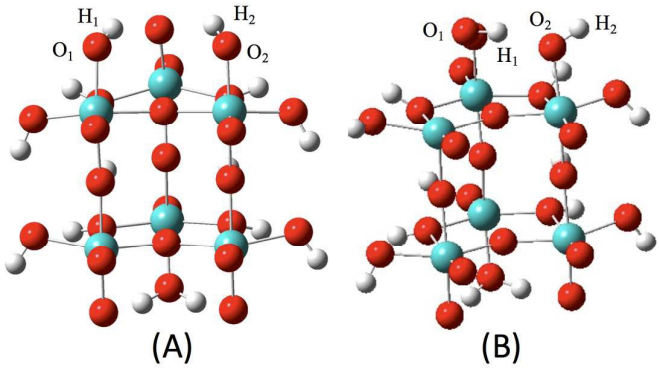

Figure 6: Dissociation structures formed by O-O bond cleavage on the $H_{0.33}MoO_3$(100) surface. Structure (A) HO-OH2, results from the migration of an OH group to a Mo atom and (B), HO-OH3, results from the migration to a surface O atom.

The second class of dissociative mechanisms for the molecular HOOH1 configuration involves O-O bond cleavage to form a final product (HO-OH2) with two OH groups attached to Mo atoms (see Figures 8 and 9). HO-OH2 (Figure 6A) is the most stable configuration studied with an adsorption energy of - 430.4 kJ/mol. Both the strong bonding between the O atoms of the peroxide and the Mo atoms (bond length of 1.87 Å) and the hydrogen bonds between the adsorbed OH species and the lattice O atoms contribute to its stability. The first O-O bond cleavage pathway to form HO-OH2 starts with an OH species migrating from the adsorbed H_2O_2 molecule to the surface lattice oxygen atom over a barrier of 124.1 kJ/mol (TS6) producing an intermediate configuration HO-OH3 (Figure 6B) with an adsorption energy of -109.2 kJ/mol. The bond length between the migrating OH group and the lattice oxygen is 1.412 Å, shorter than the bond length in the H_2O_2 molecule and the molecular absorbed species (HOOH1 and HOOH2). Another migration of the OH group through TS7 (72.3 kJ/mol) from a surface OH bonded to O atom forms HO-OH2. The initial energy barrier (TS6) is slightly larger (18.2 kJ/mol) than the adsorption energy for the HOOH1 structure. In addition, the energy of the HO-OH3 species is also slightly larger than the initial HOOH1 configuration. On a fixed cluster, TS6 is lower by 54.8 kJ/mol and the energy the HO-OH3 structure is 123.3 kJ/mol lower in energy than that of a relaxed cluster. This large energy difference between the fixed and relaxed HO-OH3 structures is partially due to stronger hydrogen bonding between H of the OH group attached to the surface oxygen and the oxygen of the OH group bonded to the surface Mo atom (1.616 Å versus 1.688 Å for the relaxed cluster). Thus, assuming the relaxation is overestimated on the relaxed cluster, this pathway could be possible on the bronze surface.

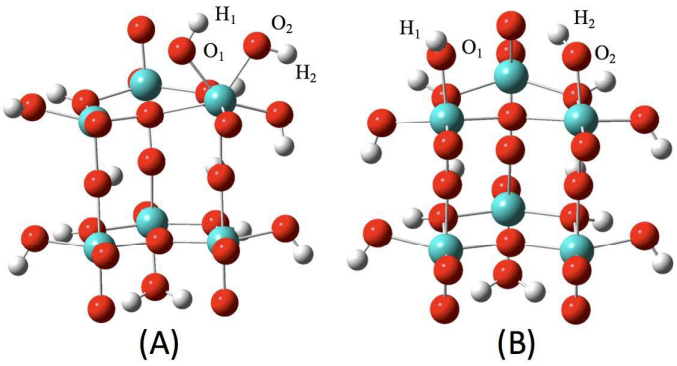

Figure 7: Additional dissociation structures formed by O-O bond cleavage on the $H_{0.33}MoO_3$(100) surface. Structure (A), HO-OH4, results from the dissociation of the O-O bond to form a geminal structure and (B), HO-OH5, results from the migration of an OH group to another surface Mo atom and is energetically close to HO-OH2.

The other O-O bond cleavage pathway from HOOH1 to HO-OH2 involves the formation of geminal Mo-$(OH)_2$ species (HO-OH4) shown in Figure 7A. Refer to Figure 9 for the the reaction steps and energetics. The reaction occurs over a barrier of 112.6 kJ/mol (TS8), 6.7 kJ/mol greater than the adsorption energy of HOOH1. Once HO-OH4 is formed, the OH group can migrate over TS9 (barrier of 60.9 kJ/mol) to form HO-OH5 (Figure 7B). The energy of this structure and the barrier (through TS10) to form the final HO-OH2 configuration are small. The analogous pathway on a fixed cluster involves the direct conversion between the HOOH1 structure and the HO-OH2 structure over a 94 kJ/mol barrier, which is less than the absorption energy of HOOH1. The lack of surface flexibility on the fixed clusters prevents the formation of a stable geminal configuration and instead favored direct

dissociation into two surface OH groups. Since the initial barrier (TS6) on the relaxed cluster is only 6.7 kJ/mol larger than the desorption energy of the HOOH1 species on the relaxed structure and the dissociation is favorable on the fixed clusters, it is also reasonable to expect that this pathway can occur on the bronze surface.

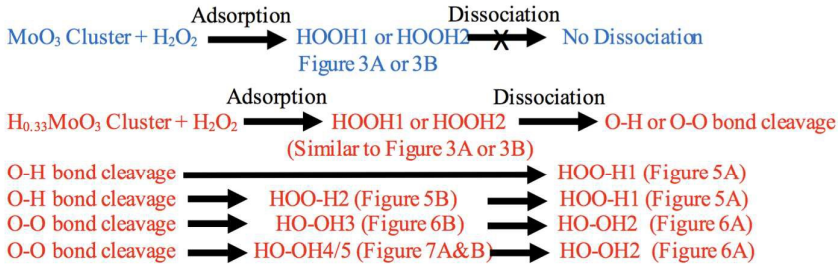

Figure 8: Overall reaction scheme for the different pathways on the MoO_3(100) and $H_{0.33}MoO_3$(100) surfaces represented by cluster models. The energies for the reactions on the $H_{0.33}MoO_3$(100) cluster are shown in Figure 9.

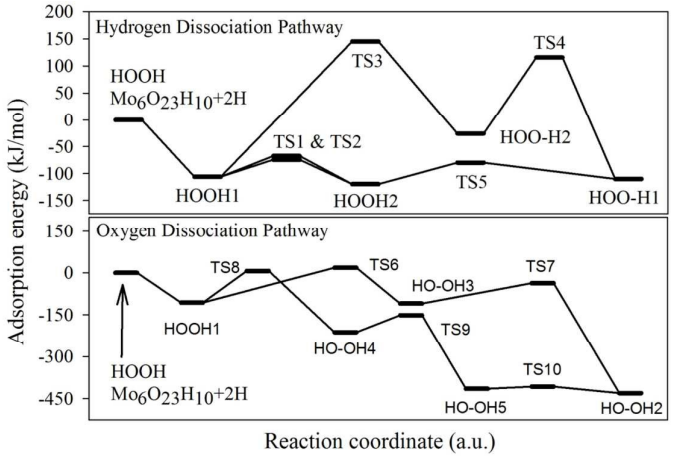

Figure 9: Energy profile for different dissociation pathways on the $H_{0.33}MoO_3$(100) surface. Energies for the stable structures can be found in Table 3, while the transition states are listed in Table 2.

Conclusions

Hydrogen peroxide can adsorb molecularly on the MoO_3(100) surface via dative bond formation between the lone pair of the oxygen atom and the empty *d*-orbital of the surface molybdenum. Consistent with the lack of electron density at the surface by the HOMO of the oxide, no dissociation is feasible. Geometry optimizations performed on configurations containing possible H_2O_2 dissociation products either led to their recombination or to a structure with a positive adsorption energy. Identical trends were found on both fixed and relaxed clusters. The addition of hydrogen atoms into the MoO_3 crystal structure results in a molybdenum bronze or $H_{0.33}MoO_3$(100) surface with a dramatically different HOMO. The existence of surface electron density provided by the HOMO on the bronze surface allows formation of strong covalent bonds between surface Mo or O atoms and H or OH species. Thus, molecularly adsorbed HOOH can dissociate into the two OH fragments or into H and OOH species on the surface. Again, the degree of relaxation of the surface of the cluster does not change this conclusion. However, there is one significant difference: on the fixed cluster one of the two molecular adsorption structures directly dissociates into an absorbed H atom and OOH group.

In the case of H_2O_2 adsorbed on the $H_{0.33}MoO_3$(100) clusters, the ultimate dissociation products are HOO-H1 via a hydrogen dissociation and HO-OH2 via an oxygen cleavage pathway. While cleaving the O-O bond in the H_2O_2 molecule to form HO-OH2 with two adsorbed OH groups results in the most energetically-favored configuration among all possible dissociated structures, the actual reaction kinetics strongly depends on the transition barrier heights. There are two possible hydrogen dissociation mechanisms. One is a direct dissociation on the relaxed cluster from either the HOOH2 structure formed by direct absorption or

from HOOH1 to form an adsorbed H atom and a OOH group through a small 39.9 kJ/mol transition barrier. As mentioned above, the HOOH2 adsorption structure dissociated directly into a H atom and a OOH group on the fixed cluster. The other hydrogen dissociation pathway involves an intermediate containing a Mo-H bond. This second pathway is unlikely due to the large transition barrier to form this intermediate (HOO-H2). The O-O bond dissociation pathway occurs either through the HOOH1 structures forming an intermediate with an OH group attached to the lattice oxygen or through an intermediate with two OH groups bound to one Mo surface atom. On the fixed cluster, the second pathway dissociates directly into the final structure due to the lack of flexibility of the surface Mo atom, which is required to form the geminal structure. Comparing the O-H bond dissociation pathways with the O-O dissociation, the O-O bond cleavage leads to the most energetically stable product, HO-OH2. However, the activation barrier for the O-H bond cleavage is significantly smaller (39.9 kJ/mol), which makes it kinetically more favorable. Given the computed energies and barriers heights, both products would be expected experimentally and a detailed study of the dynamics is required to determine the ratio between them, which is beyond the scope of this paper.

Acknowledgements

The authors acknowledge the financial support of this work by the National Science Foundation through grant ECCS-0731208. Computations for this project were partially supported by the OSU High Performance Computing Centre at Oklahoma State University, funded in part through instrumentation grant OCI–1126330 by the National Science Foundation.

Notes and References

1. J. C. Volta and J. L. Portefaix, *Appl. Catal.*, 1985, **18**, 1-32.
2. J. C. Vedrine, G. Coudurier, M. Forissier and J. C. Volta, *Catal. Today*, 1987, **1**, 261-280.
3. J. C. Volta and J. M. Tatibouet, *J. Catal.*, 1985, **93**, 467-470.
4. K. Brückman, R. Grabowski, J. Haber, A. Mazurkiewicz, J. Słoczyński and T. Wiltowski, *J. Catal.*, 1987, **104**, 71-79.
5. J. M. Tatibouët and J. E. Germain, *J. Catal.*, 1981, **72**, 375-378.
6. J. M. Tatibouet, J. E. Germain and J. C. Volta, *J. Catal.*, 1983, **82**, 240-244.
7. A. Baiker and D. Gasser, *Z Phys. Chem. Neue Fol.*, 1986, **149**, 119-124.
8. H. Al-Kandari, S. Al-Kandari, F. Al-Kharafi and A. Katrib, *Energ. Fuel*, 2009, **23**, 5737-5742.
9. in *Studies in Inorganic Chemistry*, eds. E. R. Braithwaite and J. Haber, Elsevier, 1994, vol. Volume 19, p. ii.
10. D. H. Mei, A. M. Karim and Y. Wang, *J Phys. Chem. C*, 2011, **115**, 8155-8164.
11. A. Guerrero-Ruiz, M. Abon, J. Massardier and J. C. Volta, *J. Chem. Soc., Chem. Commun.*, 1987, 1031-1033.
12. A. Papakondylis and P. Sautet, *J. Phys. Chem.*, 1996, **100**, 10681-10688.
13. A. C. Tsipis, *Phys. Chem. Chem. Phys.*, 2000, **2**, 1357-1363.
14. A. Michalak, K. Hermann and M. Witko, *Surf. Sci.*, 1996, **366**, 323-336.
15. F. Cora, A. Patel, N. M. Harrison, C. Roetti and C. Richard A. Catlow, *Mater. Res. Bull.*, 1997, **7**, 959-967.
16. D. O. Scanlon, G. W. Watson, D. J. Payne, G. R. Atkinson, R. G. Egdell and D. S. L. Law, *J Phys. Chem. C*, 2010, **114**, 4636-4645.
17. R. Coquet and D. J. Willock, *Phys. Chem. Chem. Phys.*, 2005, **7**, 3819-3828.
18. R. Tokarz-Sobieraj, K. Hermann, M. Witko, A. Blume, G. Mestl and R. Schlögl, *Surf. Sci.*, 2001, **489**, 107-125.
19. R. Tokarz-Sobieraj, M. Witko and R. Gryboś, *Catal. Today*, 2005, **99**, 241-253.
20. K. Hermann, M. Witko and A. Michalak, *Catal. Today*, 1999, **50**, 567-577.
21. C. Hoang-Van and O. Zegaoui, *Appl. Catal., A*, 1995, **130**, 89-103.
22. C. Hoang-Van and O. Zegaoui, *Appl. Catal., A*, 1997, **164**, 91-103.
23. H. Sakagami, Y. Asano, N. Takahashi and T. Matsuda, *Appl. Catal., A*, 2005, **284**, 123-130.
24. J. J. Birtill and P. G. Dickens, *Mater. Res. Bull.*, 1978, **13**, 311-316.
25. C. Ritter, W. Muller-Warmuth and R. Schollhorn, *J. Chem. Phys.*, 1985, **83**, 6130-6138.
26. P. G. Dickens, J. J. Birtill and C. J. Wright, *J Solid State Chem.*, 1979, **28**, 185-193.
27. B. Braïda, S. Adams and E. Canadell, *Chemistry of Materials*, 2005, **17**, 5957-5969.
28. X. W. Sha, L. Chen, A. C. Cooper, G. P. Pez and H. S. Cheng, *J Phys. Chem. C*, 2009, **113**, 11399-11407.
29. L. Chen, *J Phys. Chem. C*, 2008, **112**, 1755-1758.
30. K. Barber, A. W. Apblett, S. Al-Fadul, A. Piquette and M. Chehbouni, *Ceram. Trans.*, 2010, **222**, 177-187.
31. B. P. Kiran and A. W. Apblett, *Ceram. Trans.*, 2004, **155**, 371-380.
32. B. P. Kiran, A. W. Apblett and M. Chehbouni, *Ceram. Trans.*, 2003, **143**, 385-394.
33. A. W. Apblett, B. P. Kiran, S. Malka, N. F. Materer and A. Piquette, *Ceram. Trans.*, 2006, **172**, 29-35.
34. M. J. Frisch, G. W. Trucks, H. B. Schlegel, G. E. Scuseria, M. A. Robb, J. R. Cheeseman, G. Scalmani, V. Barone, B. Mennucci, G. A. Petersson, H. Nakatsuji, M. Caricato, X. Li, H. P. Hratchian, A. F. Izmaylov, J. Bloino, G. Zheng, J. L. Sonnenberg, M. Hada, M. Ehara, K. Toyota, R. Fukuda, J. Hasegawa, M. Ishida, T. Nakajima, Y. Honda, O. Kitao, H. Nakai, T. Vreven, J. A. Montgomery Jr., J. E. Peralta, F. Ogliaro, M. J. Bearpark, J. Heyd, E. N. Brothers, K. N. Kudin, V. N. Staroverov, R. Kobayashi, J. Normand, K. Raghavachari, A. P. Rendell, J. C. Burant, S. S. Iyengar, J. Tomasi, M. Cossi, N. Rega, N. J. Millam, M. Klene, J. E. Knox, J. B. Cross, V. Bakken, C. Adamo, J. Jaramillo, R. Gomperts, R. E. Stratmann, O. Yazyev, A. J. Austin, R. Cammi, C.

Pomelli, J. W. Ochterski, R. L. Martin, K. Morokuma, V. G. Zakrzewski, G. A. Voth, P. Salvador, J. J. Dannenberg, S. Dapprich, A. D. Daniels, Ö. Farkas, J. B. Foresman, J. V. Ortiz, J. Cioslowski and D. J. Fox, *Journal*, 2009.
35. A. Becke, *J. Chem. Phys.*, 1993, **98**, 5648.
36. C. T. Lee, W. T. Yang and R. G. Parr, *Phys. Rev. B*, 1988, **37**, 785-789.
37. R. Krishnan, J. S. Binkley, R. Seeger and J. A. Pople, *J. Chem. Phys.*, 1980, **72**, 650-654.
38. T. Clark, J. Chandrasekhar, G. n. W. Spitznagel and P. V. R. Schleyer, *J. Comput. Chem.*, 1983, **4**, 294-301.
39. P. J. Hay and W. R. Wadt, *J. Chem. Phys.*, 1985, **82**, 270-283.
40. P. J. Hay and W. R. Wadt, *J. Chem. Phys.*, 1985, **82**, 299-310.
41. W. R. Wadt and P. J. Hay, *J. Chem. Phys.*, 1985, **82**, 284-298.
42. S. Adams, K. H. Ehses and J. Spilker, *Acta. Crystallogr. B*, 1993, **49**, 958-967.
43. L. Kihlborg, *Ark. Kemi.*, 1963, **21**, 357-364.
44. Z. Yan, J. Fan, Z. Zuo, Z. Li and J. Zhang, *Appl. Surf. Sci.*, 2014, **288**, 690-694.
45. Z. Yan, Z. Zuo, X. Lv, Z. Li, Z. Li and W. Huang, *Appl. Surf. Sci.*, 2012, **258**, 3163-3167.
46. S. F. Boys and F. Bernardi, *Mol. Phys.*, 1970, **19**, 553-566.
47. T. H. Dunning, *J. Chem. Phys.*, 1989, **90**, 1007.
48. R. A. Kendall, T. H. Dunning and R. J. Harrison, *J. Chem. Phys.*, 1992, **96**, 6796.
49. K. A. Peterson, D. Figgen, M. Dolg and H. Stoll, *J. Chem. Phys.*, 2007, **126**, 124101.
50. S. Li, C. L. Guenther, M. S. Kelley and D. A. Dixon, *J. Chem. Phys. C*, 2011, **115**, 8072-8103.
51. S. Pudar, J. Oxgaard, K. Chenoweth, A. C. T. van Duin and W. A. Goddard, *J. Chem. Phys. C*, 2007, **111**, 16405-16415.
52. D. R. Moberg, T. J. Thibodeau, F. G. Amar and B. G. Frederick, *J Phys. Chem. C*, 2010, **114**, 13782-13795.
53. X. F. Song, G. S. Liu, H. G. Yu and A. E. Rodrigues, *J. Mol. Struc-Theochem*, 2004, **684**, 81-85.
54. S. J. Suresh and V. M. Naik, *J. Chem. Phys.*, 2000, **113**, 9727-9732.